J Solid State Electrochem (2008) 12:1511–1520
DOI 10.1007/s10008-008-0609-0

ORIGINAL PAPER

The new theory of electron transfer: application to the photosynthetic reaction centre

Stephen Fletcher

Received: 16 May 2008 / Revised: 2 June 2008 / Accepted: 2 June 2008 / Published online: 27 June 2008

Abstract Based on recent developments in the theory of electron transfer, we prove that a non-polar environment is needed to maintain the high efficiency and chemical integrity of the photosynthetic reaction centre. We also determine the Gibbs energy diagram for the primary act of charge separation in photosynthesis, and propose an equivalent circuit that captures the principal features of the entire acceptor side of the electron transport chain in photosystem II.

Keywords Electron transfer · Photosynthesis · Equivalent circuit · Gibbs energy profile · Inverted region · Electron transport chain · Marcus theory · Oxidative stress

Introduction

In two previous papers a new (non-Marcus) theory of electron transfer was developed, and the results were applied to a model system over a wide range of thermodynamic driving forces [1, 2]. In this paper, we apply the results to a real system, namely the photosynthetic reaction centre.

The new theory takes into account the fact that charge fluctuations contribute to the activation of electron transfer, besides dielectric fluctuations. When charge fluctuations are included, the results turn out to be radically different from those of previous theories, particularly those of Marcus [3–9] and Hush [10–13]. Most importantly, it is found that highly polar environments (i.e. environments having high relative permittivity) are able to catalyse the rates of thermally activated electron transfer processes, because under certain well-defined conditions they are able to stabilise the transient charges that develop on transition states. This important effect is absent from Marcus–Hush theories but is well described by the Fletcher theory [1, 2]. Some consequences of its inclusion can be seen in plots of rate constant for electron transfer versus driving force, as shown in Fig. 1. On the new theory, the relative permittivity of the environment exerts a powerful influence on the reaction rate in the highly exergonic region (the "inverted" region) and in the highly endergonic region (the "superverted" region).

Figure 1 is drawn on the assumption that electron transfer is non-adiabatic and proceeds according to Dirac's time-dependent perturbation theory [14]. Experimentally, we expect non-adiabatic electron transfer to be observed whenever there is small orbital overlap (weak coupling) between donor and acceptor states, so that overall electron transfer rates are "slow" (10 ps timescale or longer at room temperature). This encompasses most cases of biological interest.

Dirac's theory applies to any system that is undergoing a transition from one electronic state to another, in which the energies of the states are briefly equalised by fluctuations in the environment. If we assume that the relative probability of observing a fluctuation from state i to state j at temperature T is given by the Boltzmann factor $\Delta G_{ij}/k_B T$, then one finds

$$k_{et} = \frac{2\pi}{h} H_{DA}^2 \frac{1}{\sqrt{4\pi\lambda\, k_B T}} \exp\left(\frac{-(\lambda + \Delta G^0)^2}{4\lambda k_B T}\right) \quad (1)$$

where k_{et} is the rate constant for electron transfer, H_{DA} is the electronic coupling matrix element between the electron

S. Fletcher (✉)
Department of Chemistry, Loughborough University,
Ashby Road,
Loughborough, Leicestershire LE11 3TU, UK
e-mail: Stephen.Fletcher@Lboro.ac.uk

donor and acceptor species, k_B is the Boltzmann constant, λ is the reorganisation energy, and ΔG^0 is the total Gibbs energy change for the reaction. By defining a Gibbs energy of activation,

$$\Delta G^* = \frac{(\lambda + \Delta G^0)^2}{4\lambda} \tag{2}$$

we can put Eq. 1 into the standard Arrhenius form

$$k_{et} = \frac{2\pi}{\hbar} H_{DA}^2 \frac{1}{\sqrt{4\pi\lambda k_B T}} \exp\left(\frac{-\Delta G^*}{k_B T}\right) \tag{3}$$

For strongly exergonic electron transfer reactions that are activated by charge fluctuations in the environment [1, 2], the activation energy is determined by the intersection point of the following thermodynamic potentials (Gibbs energies) of the reactants and products

$$G_{\text{reactants}} = \frac{1}{2} Q_1^2 \left(\frac{1}{4\pi\varepsilon_0}\right)\left(\frac{1}{\varepsilon(0)}\right)\left(\frac{1}{a_D} + \frac{1}{a_A} - \frac{2}{d}\right) \tag{4}$$

$$G_{\text{products}} = \frac{1}{2} Q_2^2 \left(\frac{1}{4\pi\varepsilon_0}\right)\left(\frac{1}{\varepsilon(\infty) + f_1[\varepsilon(0) - \varepsilon(\infty)]}\right) \times \left(\frac{1}{a_D} + \frac{1}{a_A} - \frac{2}{d}\right) \tag{5}$$

The various terms are defined as follows. $G_{\text{reactants}}$ and G_{products} are the total Gibbs energies of the reactants and products (including their ionic atmospheres). Q_1 and Q_2 are the charge fluctuations that build up on them. $\varepsilon(0)$ is the relative permittivity of the environment in the low-frequency limit (static dielectric constant), $\varepsilon(\infty)$ is the relative permittivity of the environment in the high-frequency limit (≈2), a_A is the radius of the acceptor in the transition state (including its ionic atmosphere), a_D is the radius of the electron donor in the transition state (including its ionic atmosphere), and f_1 is a constant ($0 < f_1 < 1$) that quantifies the extent of polar screening by the environment. The term d is the distance between the electron donor and acceptor. A key prediction of Eqs. 1, 2, 3, 4, and 5 is that water is able to lower the activation energy of strongly exergonic electron transfer processes and hence catalyse them (Fig. 1).

Given the catalytic effect of polar solvents on strongly exergonic electron transfer processes, it follows that if one wants to minimise damage from such reactions inside biological membranes, then one must rigorously exclude water, which has a high relative permittivity (78) at 25 °C. In the present work, we point out that nature has contrived precisely this situation inside the photosynthetic reaction centre of plants, cyanobacteria and anoxygenic bacteria. Indeed, to inhibit photo-excited electrons from chemically reacting with nearby cofactors, scaffold proteins and membrane molecules, nature has evolved a highly non-polar, non-reducible environment inside the reductive region of photosynthetic membranes. This low-permittivity environment achieves its task by greatly increasing the electrostatic work required for electron donor and acceptor states to equalise their energies.

If nearby states readily attained the correct energies to exchange electrons, they would divert the electrons from their tunnelling pathways and—catastrophically—trigger irreversible and degenerative chemical reactions. From these telling arguments, we may therefore draw the following important conclusion: *that a non-polar environment is needed to maintain the high efficiency and chemical integrity of the solar energy harvesting system and that Darwinian evolution has converged on precisely this arrangement in all known photosynthetic species*. We further remark that such a conclusion cannot be reached by conventional Marcus theory because it predicts (erroneously) that polar environments slow down the rates of highly exergonic electron transfer reactions. In fact, the very opposite is true. Accordingly, we must reluctantly conclude that Marcus theory fails to explain electron transfer in photosynthesis [15].

Since, in our view, the photosynthetic reaction centre has evolved to make all charge fluctuations energetically unfavourable (by raising λ in Eq. 1), how then are the biologically necessary electron transfer events selectively maintained at high rates? The answer is by engineering high values of H_{DA}. This simply requires the placement of the relevant donor and acceptor states within 1.4 nm of each other, so that orbital overlap is well developed, and the tunnelling probability is high (and this is, we think, the generic reason why electron transfer in biological systems takes place through electron transport chains surrounded by hydrophobic amino acid residues).

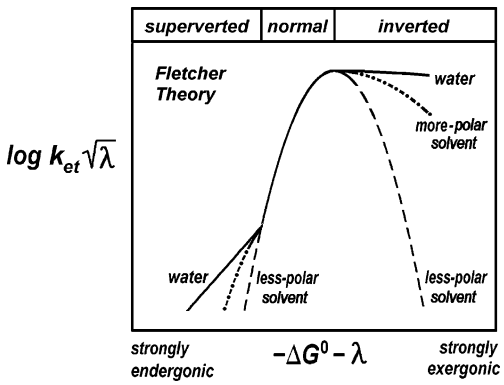

Fig. 1 The rate constant for electron transfer (k_{et}) as a function of the driving force ($-\Delta G^0$) and reorganisation energy (λ) on the Fletcher theory [1, 2]. Note the powerful catalytic effect of polar solvents (such as water) on strongly exergonic reactions

Finally, we remark that it is also desirable to exclude O_2 (oxygen) from the vicinity of the trapping states in photosynthesis [16]. This is because oxygen is readily reducible to the free radical $O_2^{\cdot-}$ ion (superoxide), which contains an unpaired electron. Although superoxide is not particularly reactive in itself, it is the precursor of a number of other oxygen-containing species that are (such as hydroxyl radicals), and these latter are known to attack double bonds or take part in hydrogen abstraction reactions [17].

The general structure of the photosynthetic reaction centre

The locus of oxygenic photosynthesis is the thylakoid. All oxygen-evolving photosynthetic organisms contain these flattened vesicles, which provide a highly structured environment in which the photosynthetic reactions take place. In plants, the thylakoid vesicles are generally housed inside larger structures called chloroplasts, which have an additional outer membrane. The solution internal to the thylakoid is referred to as the lumen, whereas the solution external to the thylakoid is referred to as the stroma. Often, to maximise the probability of light capture, thylakoids are stacked like piles of coins in structures known as grana.

Chemically, the thylakoid bilayer membranes of higher plants are composed primarily of galactolipids, which are electrically neutral (i.e. they do not have charged head groups or tail groups). Natural galactolipids are also lacking in low-lying acceptor states (i.e. they do not have conjugated double bonds). As a result of this unusual combination of features, the interior of a galactolipid membrane is electrically "quiet" (capable of only small charge fluctuations because of its low dielectric constant), non-polar (hydrophobic) and resistant to electrochemical reduction. Astonishingly, galactolipids have also evolved independently in vertebrates as components of the myelin sheath of nerves, presumably for the same electrical reasons. The structural formula of a typical chloroplast galactolipid is shown in Fig. 2.

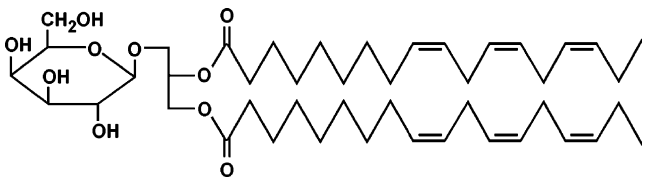

Fig. 2 Structural formula of a typical monogalactosyl diacyl glycerol that is found in thylakoid membranes. The rigorous name of the illustrated molecule is 1,2-di-(9,12,15)-octadecatrienoyl-3-*O*-β-D-galactopyranosyl-*sn*-glycerol, a widely distributed component of thylakoid membranes. The lipid tails, which we emphasise are *not* conjugated, are derived from alpha-linolenic acid (9,12,15-octadecatrienoic acid)

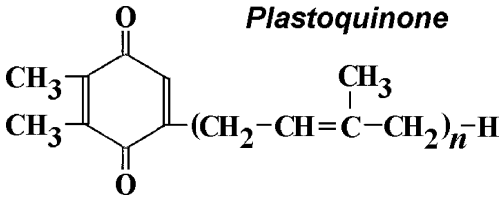

Fig. 3 Structural formula of a typical plastoquinone. The rigorous name of the illustrated molecule is 2,3-dimethyl-6-(*n*-prenyl)-1,4-benzoquinone. In most plants, $n=9$

There are four major photosynthetic complexes inside a typical thylakoid membrane: photosystem I, photosystem II, cytochrome b6f and adenosine triphosphate (ATP) synthase. Due to the large distance between PSII and the cytochrome b6f complex, various hydrophobic quinones have evolved to shuttle electrons between them without leaving the membrane. In higher plants and cyanobacteria (blue-green algae), the quinone is usually a derivative of 2,3-dimethyl-1,4-benzoquinone having an *n*-isoprenoid (*n*-prenyl) side chain (plastoquinone, see Fig. 3). In anoxygenic bacteria such as purple bacteria the corresponding quinone is usually a ubiquinone (Fig. 4). In all species, the key step is the transformation of the quinone moiety into the corresponding hydroquinone moiety by two separate electron transfer reactions.

Anoxygenic bacteria contain only one major photosystem (known as the bacterial reaction centre, bRC), but this has a number of amino acid sequences that are very similar to those in photosystem II in both plants and cyanobacteria. Indeed, it seems likely that all these photosynthetic systems evolved inside a common ancestor. One curious difference between anoxygenic bacteria and plants, however, is that their photosynthetic apparatus is located inside a cytoplasmic membrane rather than a thylakoid membrane. This suggests that the thylakoid membrane may have evolved to keep oxygen away from the reaction centre. Despite this difference in membrane chemistry, the result of exposure to light is the same in both cases; a difference of electrochemical potential $\Delta\mu$ appears across the membrane. Famously, ATP synthase exploits this electrochemical

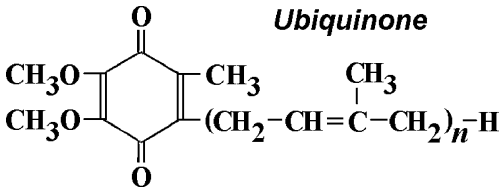

Fig. 4 Structural formula of a typical ubiquinone. The rigorous name of the illustrated molecule is 2,3-dimethoxy-5-methyl-6-(*n*-prenyl)-1,4-benzoquinone. In most anoxygenic bacteria, *n* is 8, 9 or 10

potential difference to drive the phosphorylation of adenosine diphosphate [18].

From a structural point of view, the best understood of the anoxygenic photosynthetic reaction centres are those from bacteria in the family *Rhodobacteraceae* [19, 20]. The redox cofactor organisation in the bacterial reaction centre of *Rhodobacter sphaeroides* (formerly *Rhodopseudomonas sphaeroides*) is shown in Fig. 5 [21]. A detailed picture of the mechanism of electron transfer inside the bacterial reaction centre has been built up from an epic series of experimental studies, summarised in [22–26].

The primary electron donor is a pair of bacteriochlorophyll molecules located close to the lower face of the membrane. Photoexcitation of these molecules forms a charge separated singlet state. This, in turn, triggers electron transfer to the primary quinone molecule QA via a monomeric bacteriochlorophyll (bChl) and a bacteriopheophytin (bPheo). Eventually, the photogenerated electron is passed to a secondary quinone molecule QB.

It can be seen from Fig. 5 that the redox cofactors are disposed around a twofold axis of pseudo-symmetry. The arrows indicate the pathway of light-driven electron transfer. Despite its near-symmetric form, the reaction centre behaves asymmetrically—only one of its two branches (the A-branch) actually permits high-throughput electron tunnelling [27]. The same asymmetry is found in cyanobacteria and higher plants [28]. The mechanism by which electron tunnelling is inhibited in the B-branch has not yet been discovered.

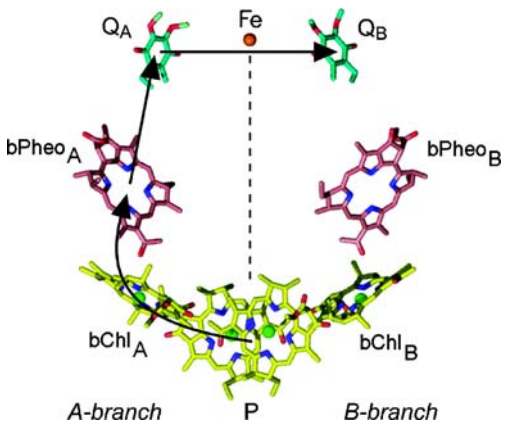

Fig. 5 Spatial organisation of electron trapping states (redox cofactors) necessary for the normal functioning of the bacterial reaction centre of the non-oxygenic purple bacterium *Rhodobacter sphaeroides*. Neighbouring states are arranged within direct electron tunnelling distance of each other (<1.4 nm). Electron transport occurs principally through the A-branch (also known as the L-branch), beginning with the pair of bacteriochlorophyll (bChl) molecules and ending with the quinone QB. The redox cofactors are kept in position by stereo-selective bonding with the helices of the A and B polypeptides. Image derived from [21]

The structure of photosystem II

We now turn our attention to photosystem II, which occurs in cyanobacteria and plants. Photosystem II is exceptional because it is the only biological machinery known that is able to oxidise water and generate molecular oxygen. In a recent series of papers, the architecture of photosystem II has been resolved at a resolution below 4.0 Å [29–31]. First, Zouni et al. elucidated the crystal structure of photosystem II from *Synechococcus elongatus* at 3.8 Å resolution [29], then Kamiya et al. reported the crystal structure of photosystem II from *Thermosynechococcus vulcanus* at 3.7 Å resolution [30]. Finally, Ferreira et al. determined the architecture of photosystem II in the cyanobacterium *Thermosynechococcus elongatus* at 3.5 Å resolution [31]. Ferreira et al. assigned all of the subunits of their photosystem II complex to specific genes and also provided a description of the protein environment of the various redox-active cofactors. In total, they assigned 3,916 residues and successfully modelled the side chains. Their work revealed the three-dimensional structure of photosystem II at very high resolution.

It turns out that photosystem II consists of about 20 different protein subunits and 14 integrally bound lipids. But, it contains only six redox cofactors that are able to trap electrons (or holes) in minima of Gibbs energy. These cofactors are the oxygen-evolving complex, the amino acid residue tyrosine (Tyr), the reaction centre chlorophyll (Chl), pheophytin (Pheo) and the plastoquinone molecules, QA and QB [32, 33]. All these cofactors except QB are bonded to a twisted pair of hydrophobic proteins known as D1 and D2. The D1 and D2 proteins form the scaffolding of the photosystem II complex. Each protein comprises five transmembrane helices (A to E) organised in a manner almost identical to that of the L and M subunits of the reaction centre of photosynthetic bacteria [34, 35]. The plastoquinone QB is exceptional in that it may either diffuse inside the membrane or bind to the reaction centre inside a special pocket. Pheo is a chlorophyll molecule lacking a central Mg^{2+} ion. The precise spatial organisation of the redox cofactors in photosystem II of *Thermosynechococcus elongatus* is shown in Fig. 6.

The Chl* excited state is delocalised over a number of chlorophyll molecules, one of which is the Chl (D1) that is involved in the initial primary charge separation. The latter molecule injects an electron into Pheo (D1). Unlike accessory BChls in the bacterial reaction centre, which are anchored by histidines, there appears to be no obvious amino acid residue to anchor Chl (D1). At the other end of the electron pathway, the full reduction of QB requires two electrons and two protons, ultimately creating the plastohydroquinone QBH_2, which diffuses into the membrane interior as a charge-neutral species. Meanwhile, a re-

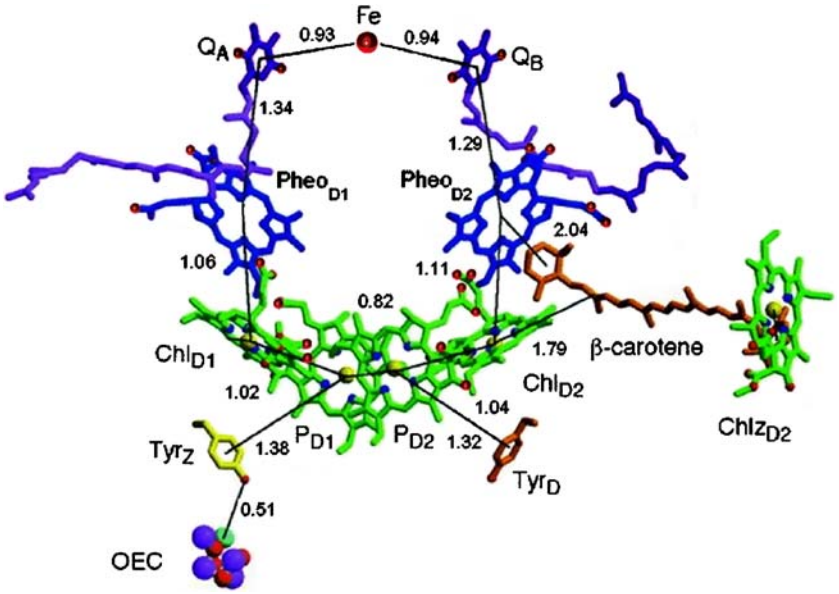

Fig. 6 Spatial organisation of redox cofactors in photosystem II of the oxygenic cyanobacterium *Thermosynechococcus elongatus*, along the internal pseudo-twofold axis. Distances in nanometres. As in the bacterial reaction centre shown in Fig. 5, all the neighbouring cofactors are arranged within electron tunnelling distance of each other (<1.4 nm). From [31]. Reprinted with permission from AAAS

oxidised QB molecule diffuses back to the binding pocket, and the process starts all over again. We can be reasonably sure that the binding pocket is connected with the polar aqueous phase (the stroma) because all the protons are sourced from there.

In our analysis that follows, the electron trapping states on the reducing side of PSII are denoted T_0, T_1, T_2, T_3 and T_4. These correspond to the redox cofactors P680, Chl*, $Pheo^-$, QA^- and QB^-, respectively. Many authors have shown that electrons tunnel spontaneously between these trapping states under the influence of an electrochemical potential $\Delta\mu$, which is generated by the absorption of light. What we now want to understand is the mechanism by which these tunnelling events occur, and how their rates are regulated.

The equivalent circuit of the electron transport chain in photosystem II

An equivalent circuit that captures the principal features of the electron transport chain in PSII is proposed in Fig. 7. At constant temperature and pressure, electrons tend to flow spontaneously from states of higher Gibbs energy to states of lower Gibbs energy, (i.e. from states of negative redox potential to states of positive redox potential). They do this provided only that (1) the lower states (electron acceptor states) are within tunnelling distance of the higher states (electron donor states), (2) thermal fluctuations are available to overcome any activation barriers between the states and (3) energetic photons do not cause the electrons to move backwards against the gradient of Gibbs potential. Two feedback modes are here included, from T_1 to T_0 (radiative decay) and from T_2 to T_0 (non-radiative decay). The existence of further feedback modes is an open question.

Above a certain threshold light level, PSII operates as a delivery-on-demand system. That is to say, the electron trapping state T_4 is filled as often as required to replenish the quinone pool. The excess electrons that make this rapid-replenishment possible must be continually drained away by an "overflow" system. This may occur radiatively via the red fluorescence or non-radiatively by a dark electron

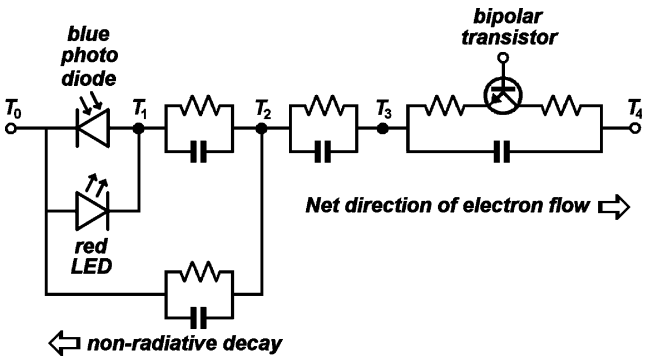

Fig. 7 Proposed equivalent circuit of the electron transport chain on the acceptor side (reducing side) of photosystem II. The electron trapping states are denoted T_0, T_1, T_2, T_3 and T_4. These correspond to the redox cofactors P680, Chl*, $Pheo^-$, QA^- and QB^-. The non-linear circuit elements (diodes and transistor) correspond to self-regulatory features of PSII. The non-radiative decay of T_2 acts as an "overflow drain" when the pathway to T_4 is full or blocked

Table 1 Approximate reversible potentials (native redox potentials measured with respect to the standard hydrogen electrode potential) and lifetimes of the trapping states in the electron transport chain of photosystem II

PSII	E_R (mV; observed)	E_R (mV; Eq. 6)	Lifetime (observed)	Lifetime (Eq. 6)
T_1 Chl	−620±100	–621	<20 ps	2 ps
T_2 Pheo	−499±100	–503	100–450 ps	200 ps
T_3 QA	−150±100	–149	100–600 μs	200 μs
T_4 QB	+50±100	+88	1 ms to 100 s	2 s

Data derived from [36–41]

transfer process, or possibly by a third mechanism as yet unknown.

In Fig. 7, the blue photodiode represents the effect of illumination on PSII. No current flows in the dark, but current flows in the light. The first stable product is a vibrationally relaxed but electronically excited state of chlorophyll (T_1). The red light-emitting diode represents the well-known energy loss from this state by fluorescence at 680 nm. To minimise this energy loss, electron tunnelling between T_1 and T_2 takes place very quickly indeed, with a time constant below 20 ps, yielding Chl^+ and $Pheo^-$. This latter species constitutes the trapping state T_2. The reversible potentials and lifetimes of all the known trapping states in PSII are summarised in Table 1.

The next act of electron transfer between $Pheo^-$ and the membrane-bound plastoquinone QA, is also surprisingly fast, having a time constant of 100–450 ps. The final act of electron transfer between the membrane-bound plastoquinone QA^- and the free plastoquinone QB is considerably slower and may be delayed still further by the time taken for free plastoquinone molecules QB to diffuse to the binding pocket or to undergo some other thermally activated process. Its time constant is not known with certainty but is probably in the range (100–600 μs). The QA/QB electron transfer process is mediated by a non-heme iron (II) atom, an arrangement that functions as a bipolar transistor, but this process is so complex that a more extensive discussion is deferred to a separate paper. The reversible potential of the QA/QA^- couple is more negative (less stable) than that of the QB/QB^- couple, doubtless because the latter is stabilised by a hydrogen-bonded (more polar) environment. Finally, to satisfy Kirchhoff's Current Law, the overall system must ultimately form a complete electrical circuit (not shown in the figure). It does this by driving protons through the membrane-spanning ATP synthase system [18].

Figure 8 is a semi-logarithmic plot of the lifetimes (τ) of various trapped species in PSII as a function of their reversible potentials E_R (volts versus SHE). The straight line is drawn according to the relation

$$(E_R/V) = 0.070 + 0.0591\ \log(\tau/s) \quad (6)$$

Due to the wide range of energies and timescales involved [36–41], the graph is robust against large measurement errors (±100 mV in potential, ± an order-of-magnitude in lifetime), so we can be confident of the general trend. It is clear that *the high energy states are the most short-lived.* Furthermore, the backward rates (on average) are about 10,000 times slower than forward rates. The electric field strength is also extraordinary—the system drops 600 mV in about 4 nm, implying a field strength of ~150 MV/m [42–43]. This is close to the dielectric breakdown strength of most cell membranes. In other words, if the field strength were slightly higher, sparks would be generated!

Gibbs energy profiles inside photosystem II

To gain a deeper insight into the operation of photosystem II, we need to construct the Gibbs energy profiles. Some general bounds on the placement of these are provided by the laws of thermodynamics. For example, on the standard hydrogen scale, the oxygen evolution reaction

$$2H_2O \leftrightarrows O_2 + 4H^+ + 4e^- \quad (7)$$

has a thermodynamic equilibrium potential of

$$E_{eq} = 1.228 - 0.0591\text{pH} + 0.0147 \log p(O_2) \quad (8)$$

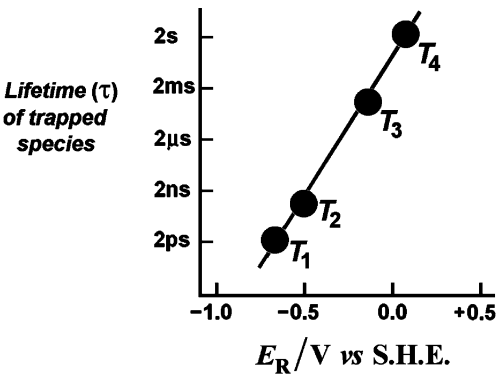

Fig. 8 The lifetimes of the trapping states in the electron transport chain of PSII as a function of their reversible potentials. Data compiled from [36–41]

at 25 °C. Thus, at pH 7.0 and 25 °C, we find that, under standard conditions, the oxidation of water (evolution of oxygen) requires E>+0.814 V. In other words, we can be sure that the Gibbs energy minimum of the Chl/Pheo/QA complex occurs at E>+0.814 V because oxygen would not be able to evolve otherwise. Here, we place the minimum at +1.114 V, since a 300 mV overpotential is comparable with the overpotential of the best metal oxide catalysts for oxygen evolution. Similarly, we can be sure that the Gibbs energy minimum of vibrationally relaxed Chl*/Pheo/QA occurs at least 1.82 V above the Gibbs energy minimum of Chl/Pheo/QA because the known fluorescence emission of PSII occurs at 680 nm (which corresponds to 1.82 eV). Furthermore, the activation energy for the charge separation step

$$\mathrm{Chl}*/\mathrm{Pheo}/\mathrm{QA} \rightarrow \mathrm{Chl}^{+}/\mathrm{Pheo}^{-}/\mathrm{QA} \quad (9)$$

must be very small because that particular reaction occurs with remarkable speed, being essentially complete within 20 ps. Gibbs energy profiles that satisfy these many and various constraints are shown in Fig. 9.

Given the known thermodynamic and kinetic constraints on PSII, there is surprisingly little leeway in the placement of the parabolas in Fig. 9. The beauty of this diagram is that the "central mystery" of photosynthesis—that is, the reason why the electron in the high-energy T_2 state does not instantaneously decay back to the low-energy ground state T_0—is now revealed. We see that there are, in fact, two activation energy barriers that inhibit this process, with the height of both barriers determined by the width of the Gibbs energy parabola of $Chl^{+}/Pheo^{-}/QA$. The situation is shown in close-up in Fig. 10. Evidently, the narrower the

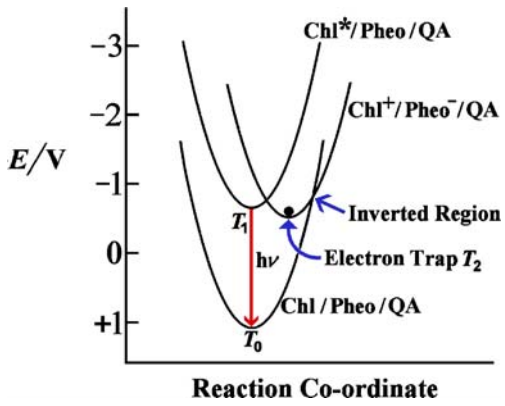

Fig. 9 Superimposed Gibbs energy profiles for different states of the Chl/Pheo/QA complex that arise inside the electron transport chain of PSII during photo-induced charge separation. The initial state is denoted Chl/Pheo/QA, the electronically excited state is denoted Chl*/Pheo/QA, and the charge-separated state is denoted $Chl^{+}/Pheo^{-}/QA$. An electron is shown in the trap T_2. The downward arrow indicates the red fluorescence emission. For clarity, we have omitted the Gibbs energy profiles of the trapping state T_3 and any triplet states

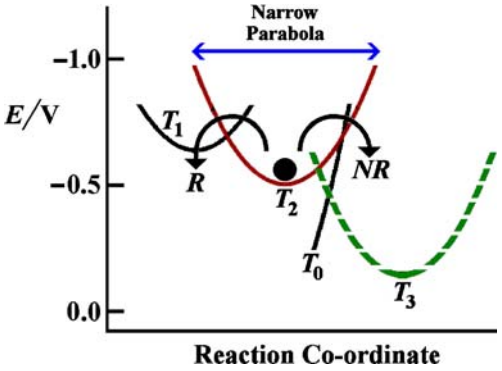

Fig. 10 Superimposed Gibbs energy profiles in the vicinity of the electron trap T_2. Trapping is thermodynamically reversible, so the electron can return to T_0 radiatively (R) via T_1 or non-radiatively (NR) via the inverted region. Both routes are kinetically hindered by the extreme narrowness of the Gibbs energy parabola, however. This narrowness is conferred by the extremely non-polar environment surrounding T_2. Trapping state T_3 is the biological goal

Gibbs energy profile, the larger the activation energies of the escape routes and the longer the lifetime of the charge-separated state T_2.

Based on recent advances in the theory of electron transfer [1, 2], we can now understand how nature manages to stabilise the charge-separated state T_2. An extremely narrow Gibbs energy parabola is formed by packing non-polar amino acid residues around it. This makes it extremely difficult for charge fluctuations to build up. Conversely, if a polar species such as water happened to encroach upon T_2, the Gibbs energy parabola would broaden in the inverted region [2], non-radiative decay would be strongly catalysed and photosynthesis would switch off. A single molecule of water might be sufficient to achieve this. Given this sensitivity to environmental polarity, it is interesting to ask if all the other trapping states in the conducting branch of PSII are surrounded by non-polar amino acid residues in a similar way. Strong evidence that this is indeed the case (based on recent X-ray data) is now presented.

The number and polarity of amino acid residues that surround the electron trapping states in photosystem II

According to recent studies of cofactor arrangements in the electron transport chain of photosystem II, the amino acid residues are arranged in the following way [29, 44].

Chl (D1) has four extremely hydrophobic phenylalanine residues in its neighbourhood (D1 Phe119, D1 Phe158, D1 Phe180 and D1 Phe182). It is also possibly hydrogen bonded via its 13(1) keto group to D2 His197 via a water molecule (although this has not yet been resolved by X-ray crystallography).

Pheo (D1) is hydrogen bonded via its 13(1) keto group to D1 Gln130 and to its ester carbonyl groups by the hydrophobic residues D1 Tyr126 and D1 Tyr147, and is also close to D2 Phe257.

The immobile quinone QA is surrounded by the hydrophobic residues D2 Ile213, D2 Met246, D2 Ala249 and D2 Ala260, and is also sandwiched between the extremely hydrophobic residues D2 Trp253 and D2 Leu267. There are also two hydrogen bonds to the oxygen atoms of the quinone headgroup, one from D2 His214 (which also ligates a non-heme iron) and one from the backbone nitrogen of D2 Phe261.

The non-heme iron (which is not a trapping state for the electron) is surrounded by D1 His215, D1 His272, D2 His214 and D2 His268. There is also a bicarbonate ion that acts as a bidentate ligand.

Finally, the mobile quinone QB resides in a binding pocket composed of yet more hydrophobic residues, including D1 Met214, D1 Leu218, D1 Ala251, D1 Phe255, D1 Phe265 and D1 Leu271. However, QB is also hydrogen bonded to D1 His215 and the side chain oxygen of D1 Ser264.

A list of amino acid residues, sorted according to the relative permittivity of their terminal functional groups, is presented in Table 2. The hydrophobicity index H is a measure of how insoluble the parent amino acid is in water. Here, we have assumed a linear correlation between the hydrophobicity of the free amino acid and the hydrophobicity of the bound amino acid. The H values in the table are normalised so that the most hydrophobic residue is given a value of 100 relative to glycine, which is arbitrarily assigned a value 0. The values below glycine are obtained by extrapolation.

Table 2 The amino acid residues that surround the electron trapping states in photosystem II, sorted according to the relative permittivity of their terminal functional groups (lowest permittivity on top)

Name		H	Location
Phenylalanine	Phe	100	D1 Phe119, D1 Phe158, D1 Phe180, D1 Phe182, D1 Phe255, D2 Phe257, D2 Phe261, D1 Phe265
Isoleucine	Ile	99	D2 Ile213
Leucine	Leu	97	D1 Leu218, D2 Leu267, D1 Leu271
Tryptophan	Trp	97	D2 Trp253
Valine	Val	76	
Methionine	Met	74	D1 Met214, D2 Met246
Tyrosine	Tyr	63	D1 Tyr126, D1 Tyr147
Alanine	Ala	41	D2 Ala249, D1 Ala251, D2 Ala260
Cysteine	Cys	49	
Threonine	Thr	13	
Histidine	His	8	D1 His215, D2 His214
Glycine	Gly	0	
Serine	Ser	−5	D1 Ser264
Glutamine	Gln	−10	D1 Gln130
Proline	Pro	−46	
Arginine (+)	Arg	−14	
Lysine (+)	Lys	−23	
Glutamic (−)	Glu	−31	
Aspartic (−)	Asp	−55	

The Hydrophobicity Index values (H) from [45]. Residue locations from [29]

Note that the highly polar carboxylic acid functional groups in each amino acid do not interfere with the electron tunnelling pathway because they are “locked up” inside peptide linkages. Phenylalanine, tryptophan and tyrosine have large aromatic ring terminations, which explains why they have very low relative permittivity (high hydrophobicity) when bonded inside proteins. They “look like benzene”. Amino acids with alkyl terminations (isoleucine, leucine, valine and alanine) also provide strong hydrophobicity inside proteins. Methionine uniquely has a chemically inert thiol ether side chain. Apart from this select group, all other amino acids have high permittivity terminations.

Among the hydrophilic amino acids, three (tyrosine, threonine and serine) have hydroxyl terminations and readily form hydrogen bonds with water. A further five have polar terminations containing lone pairs of electrons (cysteine, glycine, glutamine, histidine and proline), and these are not only hydrophilic but may also act as ligands for metal ions. Finally, four other amino acids have end groups that are electrically charged at pH 7 (arginine, lysine, glutamic acid and aspartic acid). Overall, it is clear that nature has a limited choice of amino acids for constructing pathways of low relative permittivity. Given this limited choice, it is interesting to ask which particular amino acid residues actually surround the electron trapping states in photosystem II. The results are collected in the final column of Table 2. Clearly, the majority of amino acid residues along the electron tunnelling pathway are hydrophobic, i.e. have sufficiently low permittivity to suppress unwanted side reactions. Indeed, the amino acid residues are predominantly those having alkyl or aromatic side chains, whilst those with ionic (acidic or basic) side chains are absent. These data are fully consistent with the new theory of electron transfer [1, 2].

Finally, it may be noted that, for any redox couple inside the pathway, the non-polar environment destabilises the more highly charged states, making them thermodynamically harder to form. Hence, for positively charged redox couples, such as Fe(2+)/Fe(3+), the non-polar environment causes the redox potential to shift in a positive direction. Conversely, for negatively charged redox couples, like QA/QA^{-}, the non-polar environment causes the redox potential to shift in a negative direction. This explains, in part, how PSII is able to achieve its phenomenally high oxidising and reducing potentials.

Conclusions

Photosystem II has evolved to capture solar energy efficiently and then store that energy in chemical bonds. The first step involves the photochemical excitation of stationary electrons. The second step involves the lateral tunnelling of those electrons through an electron transport chain. In the present work, we have explored the electronic structure and mechanism by which this electron transport chain operates. We find that the experimental data are consistent with a sequence of non-adiabatic electron transfer processes triggered by charge fluctuations in the environment of each electron trapping species. We can find no evidence that electron transfer is triggered by dielectric fluctuations (Marcus–Hush theory).

By the principle of least action, electrons tend to tunnel through those regions of space that have the most positive electrostatic potential. Not surprisingly, therefore, PSII has evolved a well-defined pathway of positive electrostatic potential to direct electrons to where it wants them. In the present work, we have proposed an equivalent circuit that models many of the electrical and optical features of the electron transport chain (Fig. 7). Our equivalent circuit is fully consistent with the biochemistry, electrochemistry, thermodynamics, X-ray crystal structure, femtosecond spectroscopy and quantum mechanics of PSII.

Based on recent developments in the theory of electron transfer (which, for the first time, include the role of charge fluctuations in the electron transfer process [1, 2]) and based on literature data, we have also determined the Gibbs energy diagram for the primary act of charge separation in photosynthesis. The results are shown in Figs. 9 and 10. We find that the electron resides briefly in the unstable state T_2, before moving on to the more stable state T_3. Whilst in the unstable state T_2, it may lose energy radiatively after a "normal" electron transfer process, or it may lose energy non-radiatively via an "inverted" electron transfer process. The competitive nature of these processes is evident. However, both processes are suppressed by the extreme narrowness of the Gibbs energy parabola of the T_2 state. The narrowness of the Gibbs energy parabola is conferred by the highly non-polar amino acid residues that surround the T_2 state. The resulting meta-stability of the T_2 state allows sufficient time for the electron to transfer successfully to T_3. This elegant arrangement finally explains the high efficiency of the primary charge separation step in photosynthesis.

Figure 10 also explains the well-known but puzzling experimental finding that the rate of primary charge separation in photosynthesis increases upon cooling to cryogenic temperatures. Martin and co-workers [46, 47] were the first to quantify this phenomenon by measuring the rate of electron transfer in isolated reaction centres of *Rhodobacter sphaeroides*. In the late 1980s, they found a time constant of ~2.8 ps at room temperature falling to ~1.2 ps at 10 K. Since then, the acceleration of the rate of primary charge separation by cooling has been widely confirmed [48]. Now, we have the explanation. The activation energies of the backward steps are much higher than the activation energies of the forward steps. As a consequence, the rate constants of the forward reactions are only slightly decreased by temperature, whereas their populations are greatly increased. The overall effect is an increase in rate.

An unwanted side reaction in PSII is the reduction of trace oxygen to hydrogen peroxide:

$$O_2 + e^- \leftrightarrows O_2^{\cdot -} \tag{10}$$

$$O_2^{\cdot -} + H^+ + e^- \leftrightarrows HO_2^- \tag{11}$$

$$HO_2^- + H^+ \leftrightarrows H_2O_2 \tag{12}$$

where $O_2^{\cdot -}$ is the superoxide ion and HO_2^- is the hydroperoxide ion. The overall reaction

$$O_2 + 2H^+ + 2e^- \leftrightarrows H_2O_2 \tag{13}$$

has a thermodynamic equilibrium potential

$$E_{eq} = 0.682 - 0.0591\text{pH} + 0.0295 \log\frac{p(O_2)}{[H_2O_2]} \tag{14}$$

at 25 °C. This implies that, at pH 7.0 and 25 °C and assuming $p(O_2)=10^{-6}$ and $[H_2O_2]=10^{-6}$ M, the reduction of trace oxygen may potentially occur wherever $E<+0.327$ V. The clear implication is that reactive oxygen species may form in any electron trapping state if oxygen is not excluded. It follows that oxygen and water must both be carefully regulated inside PSII if the system is to operate successfully. On the other hand, if oxygen and water enter the electron transfer pathway simultaneously, then the photosynthetic reaction centre will be subjected to powerful oxidative stress (destruction of the protein scaffold).

Regarding the overall functioning of PSII, a number of commercially available herbicides have been developed to disrupt it. One of these is 3-(3,4-dichlorophenyl)-1,1-dimethylurea (DCMU), which prevents the mobile quinone QB from docking into its binding pocket on the D1 protein. It also stimulates the chlorophyll fluorescence at 680 nm, but why? The reason is now obvious from Fig. 7. When DCMU blocks electron flow, the occupancy of the T_1 state increases and the red fluorescence is stimulated. Conversely, when DCMU is removed, the occupancy of the T_1 state decreases and the red fluorescence is quenched. By similar

reasoning, the addition of oxidised QB should enhance the electron flow, decrease the occupancy of the T_1 state and therefore quench the chlorophyll fluorescence. This is exactly what is observed experimentally [49].

Finally, we conclude that the asymmetric conductance of the near-symmetric reaction centre (Fig. 5) has almost certainly evolved to prevent the highly reactive semiquinone intermediate $QA^{\cdot-}$ from physically escaping. Thus, natural selection has sacrificed the photochemical functioning of the D2 branch of photosystem II (*B*-branch of the bacterial reaction centre) in order to construct a semiquinone trapping state at the point where the photogenerated electrons exit the reaction centre. This strategy undoubtedly has a strong survival advantage because it prevents the proliferation of unwanted free radical reactions involving $QA^{\cdot-}$. Originally, the non-heme Fe(II) atom may perhaps have allowed the stabilisation of the unpaired electron over two QA molecules. But, today it clearly functions as an "electron window" (superexchange conduit) between the trapped QA and the free QB.

Acknowledgment I should like to thank Christian Amatore (École Normale Supérieure, Paris) for drawing the problem of charge transfer in PSII to my attention, and Frank Müh (Freie Universität, Berlin) and Athina Zouni (Technische Universität, Berlin) for their generous help in interpreting the X-ray crystal structures of PSII.

References

1. Fletcher S (2007) J Solid State Electrochem 11:965
2. Fletcher S (2008) J Solid State Electrochem 12:765
3. Marcus RA (1956) J Chem Phys 24:966
4. Marcus RA (1956) J Chem Phys 24:979
5. Marcus RA (1963) J Chem Phys 38:1858
6. Marcus RA (1964) Ann Rev Phys Chem 15:155
7. Marcus RA (1965) J Phys Chem 43:679
8. Marcus RA (1994) J Phys Chem 98:7170
9. Marcus RA (1997) Electron transfer reactions in chemistry: theory and experiment. In: Malmström BG (ed) Nobel lectures, chemistry 1991–1995. World Scientific Publishing, Singapore
10. Hush NS (1961) Proceedings of the Fourth Moscow conference of electrochemistry (1956). Consultants Bureau, New York (English translation 1961)
11. Hush NS (1958) J Chem Phys 28:962
12. Hush NS (1961) Trans Faraday Soc 57:557
13. Hush NS (1999) J Electroanal Chem 470:170
14. Dirac PAM (1930) The principles of quantum mechanics. Clarendon, Oxford
15. Marcus RA, Sutin N (1985) In: Michel-Beyerle ME (ed) Antennas and reaction centers of photosynthetic bacteria. Springer, Berlin, West Germany, pp 226–233
16. Khorobrykh S, Mubarakshina M, Ivanov B (2004) Biochim Biophys Acta 1657:164
17. Afanas'ev IB (1991) Superoxide ion: chemistry and biological implications. CRC, Boca Raton, FL
18. Mitchell P (1961) Nature 191:144
19. Deisenhofer J, Norris JR (eds) (1993) The photosynthetic reaction centre, vols. I and II. Academic, San Diego, CA
20. Blankenship RE, Madigan MT, Bauer CE (eds) (1995) Anoxygenic photosynthetic bacteria. Kluwer, Dordrecht, The Netherlands
21. Wakeham MC, Jones MR (2005) Biochem Soc Trans 33:851
22. Woodbury NW, Allen JP (1995) In: Blankenship RE, Madigan MT, Bauer CE (eds) Anoxygenic photosynthetic bacteria. Kluwer, Dordrecht, The Netherlands, pp 527–557
23. Parson WW (1996) In: Bendall DS (ed) Protein electron transfer. BIOS Scientific Publishers Ltd, Oxford, pp 125–160
24. Hoff AJ, Deisenhofer J (1997) Phys Rep 287:1
25. Okamura MY, Paddock ML, Graige WS, Feher G. (2000) Biochim Biophys Acta 1458:148
26. Wraight CA (2004) Front Biosci 9:309
27. Vermeglio A, Clayton RK (1977) Biochim Biophys Acta 461:159
28. Bouges-Bocquet B (1973) Biochim Biophys Acta 314:250
29. Zouni A, Witt HT, Kern J, Fromme P, Krauss N, Saenger W, Orth P (2001) Nature 409:739
30. Kamiya N, Shen J-R (2003) Proc Natl Acad Sci U S A 100:98
31. Ferreira KN, Iverson TM, Maghlaoui K, Barber J, Iwata S (2004) Science 303:1831
32. Debus R (1992) Biochim Biophys Acta 1102:269
33. Klimov VV (2003) Photosynth Res 76:247
34. Deisenhofer J, Epp O, Miki K, Huber R, Michel H (1985) Nature 318:618
35. Allen JP, Feher G, Yeates TO, Komiya H, Rees DC (1988) Proc Natl Acad Sci U S A 85:8487
36. Orr L, Govindjee (2007) Photosynth Res 91:107
37. Ishikita H, Biesiadka J, Loll B, Saenger W, Knapp E-W (2006) Angew Chem Int Ed 45:1964
38. Ishikita H, Saenger W, Biesiadka J, Loll B, Knapp E-W (2006) Proc Natl Acad Sci U S A 103:9855
39. Johnson GN, Rutherford AW, Krieger A (1995) Biochim Biophys Acta (Bioenergetics) 1229:202
40. Klimov VV, Krasnovskii AA (1981) Photosynthetica 15:592
41. Diner BA, Rappaport F (2002) Ann Rev Plant Biol 53:551
42. Tanaka S, Marcus RA (1997) J Phys Chem B 101:5031
43. Marcus RA, Sutin N (1985) Biochim Biophys Acta (Reviews on Bioenergetics) 811:265
44. Loll B, Kern J, Saenger W, Zouni A, Biesiadka J (2005) Nature 438:1040
45. Monera OD, Sereda TJ, Zhou NE, Kay CM, Hodges RS (1995) J Pept Sci 1:319
46. Martin J-L, Breton J, Hoff AJ, Migus A, Antonetti A (1986) Proc Natl Acad Sci U S A 83:957
47. Breton J, Martin J-L, Fleming GR, Lambry J-C (1988) Biochemistry 27:8276
48. Aartsma TJ, Amesz J (1996) Photosynth Res 48:99
49. Kurreck J, Schödel R, Renger G (2000) Photosynth Res 63:171